Comparison of the photothermal sensitivity of an interferometric optical fiber probe with pulsed photothermal radiometry

J. G. Laufer, P. C. Beard, and T. N. Mills
Department of Medical Physics and Bioengineering, University College London, 11-20 Capper Street, London WC1E 6JA, United Kingdom

(Received 22 January 2002; accepted for publication 4 June 2002)

An interferometric optical fiber probe for making photothermal measurements of tissue optical and thermal properties is compared to pulsed photothermal radiometry in terms of its overall thermal sensitivity, linearity, and response time. The principles of operation of the probe are described and its performance as a low finesse Fabry–Perot interferometer is discussed. A probe with a 12 μm sensing film is characterized by a thermal noise floor of 50 mK and a response time of 850 μs. The sensitivities to the optical and thermal coefficients of the two techniques have been analyzed. As a result of the different source geometries, the optical fiber probe was found to be more sensitive to the thermal coefficients of tissue than the optical coefficients while pulsed photothermal radiometry provided maximum sensitivity to the optical coefficients. © *2002 American Institute of Physics.* [DOI: 10.1063/1.1499759]

I. INTRODUCTION

Pulsed photothermal techniques have been applied to many areas ranging from material science[1–3] to the characterization of biological media[4–6] and rely on the detection of the time-dependent temperature changes following the absorption of a pulse of optical energy. The amplitude and temporal characteristics of the photothermal signals depend upon the optical and thermal properties as well as the illumination geometry of the target. By interpreting the detected photothermal response using theoretical models of photothermal signal generation, the optical and thermal coefficients of a material can be determined.

Pulsed photothermal radiometry (PPTR) has been used for the determination of optical[7] and optothermal[8] coefficients of tissue and for the characterization of skin.[9,10] PPTR, which relies on the detection of infrared emissions from a target following the absorption of a pulse of optical energy, is widely used in material science and can perhaps be described as a gold standard technique. PPTR does, however, have limitations since the free-space detection of infrared emissions requires optical components that would be too large to allow endoscopic or interstitial measurements. The use of infrared transmitting fibers, which could overcome this limitation, can suffer from disadvantages such as photodegradation and low damage thresholds of such fibers. An interferometric optical fiber probe has been developed with the aim of detecting of cancer and other tissue pathologies.[11] In contrast to PPTR, the small size of the probe would allow photothermal measurements to be made endoscopically or interstitially deep inside the human body. The diagnosis would be based upon differences in the optical coefficients of tissue determined from photothermal measurements.

In this article, the performance of the optical fiber probe is compared with that of PPTR. The ability of the optical fiber probe and PPTR to resolve differences in absorption coefficient, reduced scattering coefficient, and thermal coefficients using numerical and analytic models of the photothermal signal generation is discussed.

In Sec. II, the principles of operation of the interferometric optical fiber probe are introduced and its performance as a low finesse Fabry–Perot interferometer and temperature sensor is discussed. In Sec. III, the thermal response of the probe is compared to that of a mercury–cadmium–telluride (HgCdTe) radiometric detector in terms of its linearity, response time, and thermal sensitivity. The sensitivity of both techniques to the optical and thermal coefficients is analyzed in Sec. IV.

II. PHOTOTHERMAL OPTICAL FIBER PROBE: THEORY AND PRINCIPLES OF OPERATIONS

The sensor consists of a thin transparent polymer film acting as a low finesse Fabry–Perot interferometer as shown in Fig. 1. The film is positioned in front of the distal end of a multimode optical fiber and is illuminated by the cw output of a tunable diode laser. The distal end of the fiber and the sensing film are separated by a water cavity producing similar reflection coefficients on either side of the film for maximum fringe visibility and hence sensitivity. The refractive index mismatches at the faces of the film produce small Fresnel reflections, which are transmitted back along the fiber to a photodiode for detection. The sensing film is in thermal contact with the target. A photothermal signal is generated by the transmission of a laser pulse through the optical fiber and the sensing film to be absorbed in the target. The absorbed optical energy, the distribution of which depends upon the optical and thermal coefficients of the target, produces an abrupt temperature rise. The subsequent axial heat flow towards the optical fiber and radial heat flow into the adjacent regions produce time-dependent thermally induced changes in the optical thickness of the film. This results in a variation in the phase shift between the two interfering reflections and a corresponding time-varying modulation in the

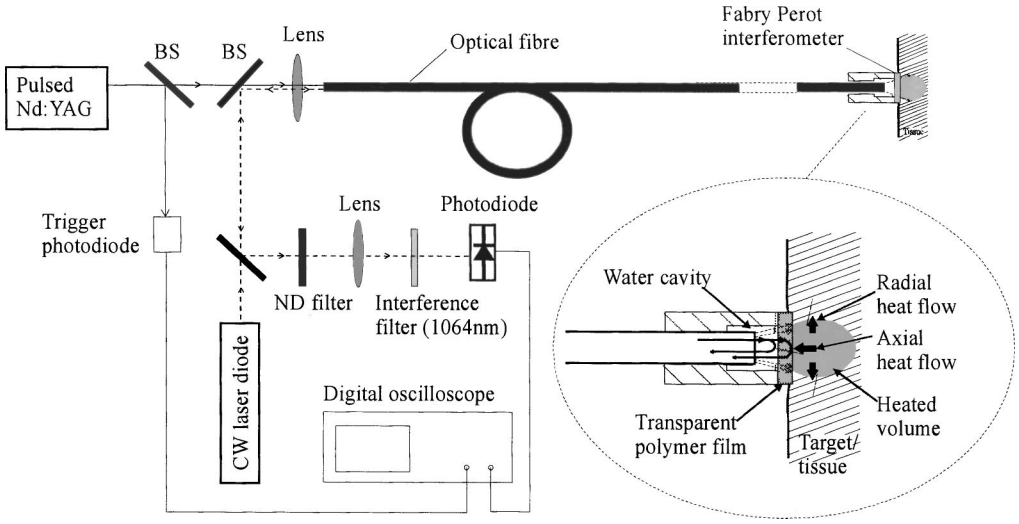

FIG. 1. Experimental configuration of the optical fiber probe.

optical power incident on the photodiode. Thermally induced changes in optical thickness are due to thermal expansion and the temperature dependence of the refractive index, known as the thermo-optic effect. A near linear response in reflected intensity is obtained for small (<0.35 rad) thermally induced phase shifts by setting the phase bias of the Fabry–Perot interferometer to the so-called quadrature point. This is the phase bias at the point of maximum slope on the interferometer transfer function and is obtained by tuning the wavelength of the laser source. The optical and thermal coefficients of the target can be determined by fitting a numerical model of photothermal signal generation to the detected response.[11] In the following subsections, the operating principles and the performance of the optical fiber probe as a Fabry–Perot interferometer are discussed.

A. Output of the low finesse Fabry–Perot interferometer

A transparent polymer film of thickness l and refractive index n is the sensing element of the optical fiber probe and acts as a Fabry–Perot interferometer. The film is bounded on either side by media of refractive indices n_1 and n_2 as shown in Fig. 2.

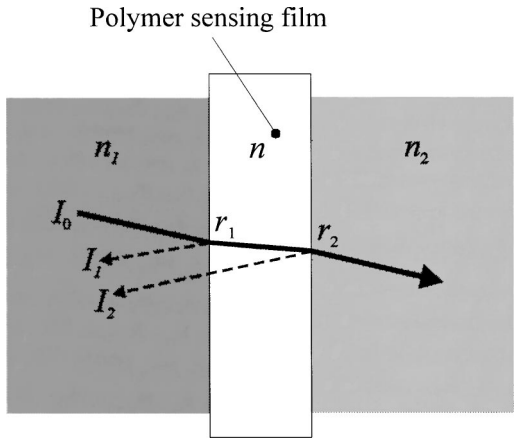

FIG. 2. Polymer sensing film acting as a low finesse interferometer.

The total reflected intensity I is given as[12]

$$I = I_1 + I_2 + 2\sqrt{I_1 I_2}\cos\phi. \tag{1}$$

This yields an expression for the phase sensitivity, defined as the change in intensity dI due to a small change in optical phase $d\phi$ from an initial quadrature phase bias point, and is given by[12]

$$\frac{dI}{d\phi} = 2I_0(1-r_1)\sqrt{r_1 r_2}, \tag{2}$$

where the reflection coefficients r_1 and r_2 are defined as

$$r_1 = \left(\frac{n-n_1}{n+n_1}\right)^2 \quad \text{and} \quad r_2 = \left(\frac{n-n_2}{n+n_2}\right)^2. \tag{3}$$

The output of the Fabry–Perot interferometer also contains a dc component, I_{dc}, given as

$$I_{dc} = I_0[r_1 + (1-r_1)^2 r_2]. \tag{4}$$

The assumption of a change in intensity with phase modulation with a deviation of less than 3% from a linear function is valid for $d\phi < 0.35$ rad. It can be seen from Eq. (2) that the phase sensitivity is dependent upon I, r_1, and r_2 and can be optimized through deliberate selection of the three parameters. These parameters also affect the dc component of the reflected light, which is an undesirable part of the interferometer output. A high dc level may saturate the photodiode, thereby limiting the maximum phase sensitivity that can be achieved. A large photocurrent would also produce increased shot noise, which would worsen the noise characteristics of the photodiode and reduce the overall sensitivity of the probe. It is therefore advantageous to maximize the phase sensitivity while minimizing I_{dc}. The optimum is achieved when the fringe visibility M, which is given as[13]

$$M = \frac{I_{max} - I_{min}}{I_{max} + I_{min}} = \frac{2I_0(1-r_1)\sqrt{r_1 r_2}}{I_0[r_1 + (1-r_1)^2 r_2]}, \tag{5}$$

is equal to one. For the case of a low finesse interferometer, this requires r_1 and r_2 to have the same value. This can be achieved by bringing both sides of the polymer film in con-

tact with material of similar refractive index. In the case of the optical fiber probe discussed here, the reflection coefficients at the polymer–tissue and polymer–water interface produce an almost optimal fringe visibility since the refractive index of tissue in the visible and near-infrared wavelength region ($n \sim 1.4$) is similar to that of water ($n = 1.33$). Maximum phase sensitivity can then be achieved by increasing I_0 to just below the saturation threshold of the photodiode. The optical fiber probe was configured with a polyethylene terephthalate (PET) film with a refractive index of $n_{\mathrm{PET}} = 1.65$, which provided sufficiently high reflection coefficients. For a PET film surrounded by water ($n_1 = n_2 = 1.33$) illuminated by an intensity $I = 1$ mW, a phase sensitivity $dI_0/d\phi = 21.6\ \mu\mathrm{W\,rad^{-1}}$ is produced. This figure could be further increased by using film materials of higher refractive index, such as diamond ($n = 2.4$). A diamond film would yield a phase sensitivity of 155 $\mu\mathrm{W\,rad^{-1}}$. However, the PET film was chosen since it produced adequate phase sensitivity and was available in different thicknesses of good optical quality. Diamond would nevertheless be a very interesting material for photothermal measurements due to its high thermal conductivity, which would result in a faster thermal detector compared to PET.

So far, the interferometer output has been analyzed for light at a single angle of incidence. In the optical fiber probe, the sensing film is illuminated by a divergent beam from a multimode optical fiber, which results in a variety of optical path lengths and hence phase biases. The effect of the divergent beam can be neglected however, since it has been shown[14] that phase dispersion, which would otherwise degrade the fringe visibility, is low for small cavity thickness ($<20\ \mu$m) and low beam divergence ($<4°$). These conditions were fulfilled by using a 12 μm polymer film and a low numerical aperture fiber (NA<0.12).

B. Thermal phase sensitivity

The static phase bias ϕ for normal incidence between the reflections is given as[13]

$$\phi = \frac{4\pi n l}{\lambda}, \tag{6}$$

where l is the thickness of the film and λ is the wavelength of the incident light. A temperature change dT in the film causes a change dl due to thermal expansion and a change dn due to the thermo-optic effect. Equation (6), differentiated with respect to T, yields an expression for the thermal phase sensitivity, defined as

$$\frac{\Delta\phi}{\Delta T} = \frac{4\pi n l}{\lambda}\left(\frac{1}{l}\frac{dl}{dT} + \frac{1}{n}\frac{dn}{dT}\right), \tag{7}$$

where $l^{-1}\ dl/dT$ is the linear thermal expansion coefficient and dn/dT is the temperature coefficient of the refractive index or thermo-optic coefficient. Heat propagating through the film induces a change in thickness and refractive index which give rise to a phase modulation $\Delta\phi/\Delta T$. The thermal phase sensitivity is therefore determined by n, l, and their temperature coefficients. The thermal phase sensitivity could be maximized by choosing a material of high film thickness and refractive index as well as high thermal expansion and thermo-optic coefficients. The drawback could be a long response time if the film materials is of low thermal conductivity. The optical fiber probe, however, was required to detect relatively fast thermal transients in tissue phantoms. A 12 μm PET film provided an adequate compromise between thermal phase sensitivity and response time.

C. Overall system sensitivity

The overall system sensitivity is obtained by multiplying Eqs. (2) and (7) and relates the change in temperature to a change in reflected intensity:

$$\frac{\Delta I}{\Delta T} = \frac{8\pi n l I_0 (1-r_1)\sqrt{r_1 r_2}}{\lambda}\left(\frac{1}{n}\frac{dn}{dT} + \frac{1}{l}\frac{dl}{dT}\right). \tag{8}$$

III. COMPARISON OF THE THERMAL RESPONSE OF THE OPTICAL FIBER PROBE WITH A HgCdTe DETECTOR

The performance of the optical fiber probe is compared to that of photoconductive mercury–cadmium–telluride (HgCdTe) detectors, which have been widely used in PPTR for the determination of optical coefficients of tissue and tissue phantoms. As photonic semiconductor devices they are characterized by fast response times and high sensitivity,[15] and provide a gold standard to which the optical fiber probe is compared. The radiometric sensitivity of a HgCdTe detector increases with active area but this improvement is accompanied by an increase in the response time. The PPTR setup used for the results reported below was similar to that employed for a number of previous studies on tissue[5] and tissue phantoms.[6,7]

A. System sensitivity

The thermal sensitivity of the optical fiber probe was measured by placing the sensor head in a water bath at a temperature of 50 °C. The probe output was recorded while the water was allowed to cool. The water temperature was measured simultaneously using a thermocouple that was positioned close to the sensing film. The thermal sensitivity was obtained from the linear regression through the data gathered for temperatures between 0 and 20 K above ambient. The thermal noise floor was calculated from the measured thermal sensitivity and the noise of the optical detection system. The overall system noise consisted of detector noise arising from the photodiode and the transimpedance amplifier as well as laser noise due to intensity and frequency fluctuations. The thermal noise floor of the probe configured with a 12 μm PET sensing film was measured as 50 mK using 32 signal averages over a bandwidth of 10 kHz. The largest contribution to the overall system noise came from low frequency intensity fluctuations of the diode laser.

The sensitivity of the optical fiber probe could be improved in a number of ways. As was described in Sec. II B, the thermal phase sensitivity could be maximized by using sensing films of greater thickness, higher refractive index, and greater thermal expansion and thermo-optic coefficient. An increase in film thickness, however, may also reduce the response time as will be shown in Sec. III C. The system

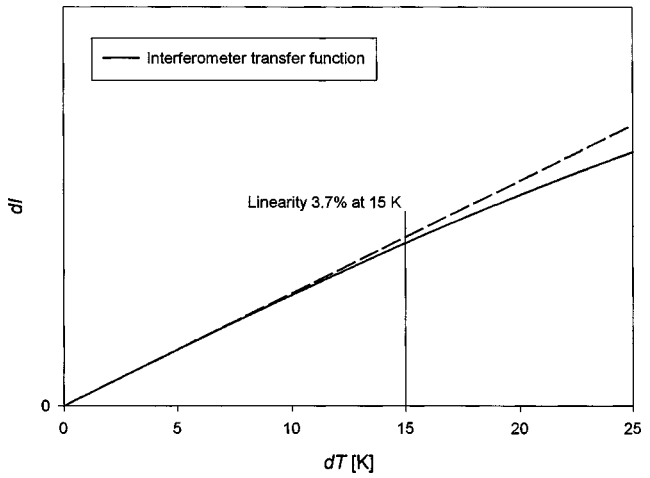

FIG. 3. The output of the Fabry–Perot interferometer with a cavity thickness of 12 μm compared to a linear function for small temperature changes.

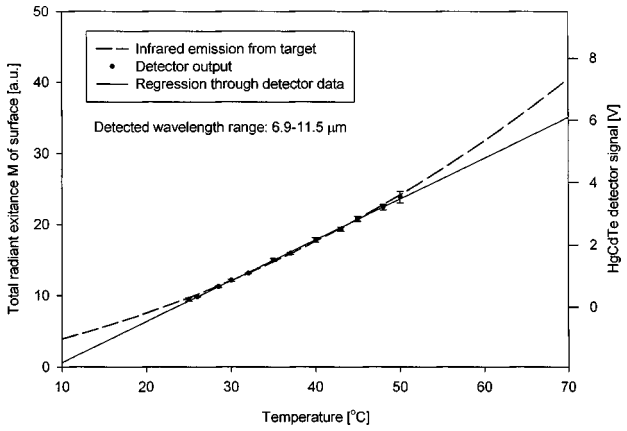

FIG. 4. The output voltage of the HgCdTe detector vs temperature shown in comparison with the equivalent change in radiant excitance of a blackbody.

sensitivity can also be improved by using laser diodes with lower intensity noise. Radiometric detection systems using HgCdTe detectors have been reported to yield minimum detectable temperature changes of <1 mK.[16] HgCdTe detectors, therefore, yield higher sensitivity than the optical fiber probe. However, by exploiting the above mentioned options to maximize the performance of the probe, similar sensitivity to HgCdTe detectors could, in principle, be achieved.

B. Linearity

The interferometer transfer function of a low finesse Fabry–Perot interferometer, which expresses the dependence of the reflected intensity on the phase shift, is a sinusoidal function and therefore inherently nonlinear. However, if the interferometer is biased at the quadrature point and the measured-induced phase shifts are suitably small, an acceptable degree of linearity can be obtained. To assess this, a previously obtained experimental value for $d\phi/dT$[17] for a PET sensing film was used to calculate the phase shift for a range of temperatures and then, from Eq. (1), the corresponding change in intensity was obtained. This is shown in Fig. 3 and indicates that the sensor is linear to within 4% over a temperature range of 15 K. This was also confirmed experimentally by measuring the probe output, which was near linear for a temperature increase of up to 20 K.

The output of a HgCdTe detector (Fermionics, PC-12-1) was measured using a graphite block as a blackbody source, which was heated electrically to a maximum temperature of 50 °C. The temperature of the graphite was measured using an embedded thermocouple. The emissions from the graphite rod was focused on to the active area of the HgCdTe detector using a Si lens.

For intensities below the saturation threshold, the output of a HgCdTe detector as a function of intensity of infrared radiation can be assumed linear. However, the radiation incident on a HgCdTe detector is not linear with the blackbody temperature as shown in Fig. 4. This is due to the shift of the maximum blackbody emittance towards shorter wavelengths according to Wien's displacement law. Typical HgCdTe detectors are sensitive to infrared wavelengths between 3 and 12 μm. Changes in the temperature of a blackbody emitter affect shorter wavelengths more strongly than the longer wavelength. This contributes to a nonlinear output for large temperature variations. The effect can be regarded as negligible, however, for small temperature changes. Figure 4 shows that a linear detector output can be assumed for temperature changes of up to 25 K above ambient.

C. Response time

The response time t of the sensing film of the probe can be estimated from heat conduction theory.[18] Equation (9) is an expression for the time t it takes the temperature at a distance l in a semi-infinite solid to reach $1-e^{-1}$ of the surface temperature at $t=0$ following a step change in the temperature at the surface. t is a measure of the sensor response time because it represents the time during which heat diffuses across a slab:

$$t=\frac{l^2\rho c}{2k}, \tag{9}$$

where l is the sensing film thickness, ρ is the density, c is the specific heat, and k is the conductivity of the polymer. For a 12 μm PET film ($\rho=1.37\times10^{-3}$ g mm^{-3}, $c=1.25$ J g^{-1} K^{-1}, $k=0.29\times10^{-3}$ W mm^{-1} K^{-1}),[19] t is 850 μs. HgCdTe detectors with a typical bandwidth of 2 MHz produce a response time of 0.5 μs and are therefore much faster than the optical fiber probe. The response time of the optical fiber probe is longer than that of HgCdTe detectors since it is determined by the speed of thermal conduction in the sensing film. The probe response time can be decreased by using materials with high thermal conductivity or by decreasing the film thickness. Reducing the film thickness, however, would adversely affect the thermal phase sensitivity unless materials of high refractive index or high thermal expansion and thermo-optic coefficients were used.

IV. COMPARISON OF THE SENSITIVITY OF THE OPTICAL FIBER PROBE AND PULSED PHOTOTHERMAL RADIOMETRY TO OPTICAL AND THERMAL COEFFICIENTS

In previous studies, the optical fiber probe and PPTR have been applied to the photothermal determination of optical coefficients of tissue phantoms.[11,20] For signals detected using the probe, a numerical model[11] was employed to extract the optical coefficients while an analytic theory[6] was utilized for PPTR signals. PPTR differs fundamentally from the optical fiber probe in terms of the thermal geometry and the principles of photothermal detection, which is reflected in their relative sensitivity to optical and thermal coefficients. In this section, the sensitivity of the optical fiber probe is compared to that of PPTR.

A. Modeling of photothermal signals

The modeling of photothermal signal generation requires solving the heat conduction equation[18] in order to describe the heat transfer in the target and the probe after the absorption of a pulse of optical energy. For PPTR, analytic solutions to the partial differential heat conduction equation that model the infrared photothermal response can be obtained.[6] In PPTR, which relies upon the detection of blackbody infrared emissions from a target following the absorption of a pulse of optical energy, an infrared detector is positioned at the focus of either an ellipsoidal mirror or a lens, while the other focus is located at the center of the target area illuminated by the optical pulse. Providing the lateral dimensions of the irradiated target area are large compared to the optical penetration depth, thermal diffusion length, and the dimensions of the detection area, a one-dimensional thermal geometry is created. This ensures that the detected photothermal signal represents the change in surface temperature due to heat flow in the direction orthogonal to the surface, which allows analytic models for the interpretation of PPTR signals to be obtained. In a number of studies,[6,21,22] expressions for PPTR signals have been derived from the heat conduction equation for specific boundary conditions using analytic descriptions of light transport in the target, which were used to calculate the initial distribution of optical energy and hence temperature in the target. Light transport was usually described using the Lambert–Bouguer law or the diffusion approximation of the radiative transport equation. The analytic expressions of the PPTR signal were then fitted to the experimental data to determine the optical or thermal coefficients of the target material. Such a theory, developed by Prahl *et al.*[6] for the determination of μ_a and μ_s' of tissue from PPTR signals, is used here to assess the sensitivity of the technique to the optical and thermal coefficients of the target. Prahl's expression for the calculation of PPTR signals detected in turbid media is given here for completeness:

$$S(t)=C\frac{\mu_a\mu_{\mathrm{IR}}}{\rho c}\left(\begin{array}{l}\dfrac{A}{\mu_{\mathrm{IR}}^2-\mu_{\mathrm{eff}}^2}[\mu_{\mathrm{IR}}f(\mu_{\mathrm{eff}}^2\alpha t)+\mu_{\mathrm{eff}}f(\mu_{\mathrm{IR}}^2\alpha t)]\\ +\dfrac{B}{\mu_{\mathrm{IR}}^2-\mu_{\mathrm{eff}}^2}[\mu_{\mathrm{IR}}f(\mu_{\mathrm{tr}}^2\alpha t)+\mu_{\mathrm{tr}}f(\mu_{\mathrm{IR}}^2\alpha t)]\end{array}\right) \tag{10}$$

with

$$A=\frac{E_{\mathrm{inc}}(9+6k)\mu_s'D}{(1+k\sqrt{4\mu_aD})(1-9\mu_aD)}\quad B=\frac{-2E_{\mathrm{inc}}}{(1-9\mu_aD)}, \tag{11}$$

where $f(x)=\exp(x)\mathrm{erfc}(x^{1/2})$ with $\mathrm{erfc}(x)$ the complimentary error function[23] of x, $\mu_s'=\mu_s(1-g)$ is the reduced scattering coefficient, g the average cosine of the scattering angle, $\mu_{\mathrm{tr}}=\mu_a+\mu_s'$ the transport coefficient, $k=(1+r_d)/(1-r_d)$ is a constant which depends on the internal diffuse reflection coefficient r_d of the target, $D=(3\mu_{\mathrm{tr}})^{-1}$ is the optical diffusion constant, $\alpha=kc^{-1}\rho^{-1}$ is the thermal diffusivity, and $\mu_{\mathrm{eff}}=(3\mu_{\mathrm{tr}}\mu_a)^{1/2}$ is the effective attenuation coefficient.

The optical fiber probe on the other hand possesses identical areas of photothermal excitation and detection, which resulted in a thermal geometry where the signal was a combination of heat flow through the sensing film along the central axis of the probe as well as radial heat flow to the sides of the heated volume (Fig. 1). The process of heat conduction is therefore a two-dimensional problem, which made numerical methods the preferred choice for the modeling of heating conduction since analytic solutions would have been difficult to derive. The model of photothermal signal generation used was a combination of models of light transport for the calculation of the initial temperature distribution, such as the Lambert–Bouguer law or the Monte Carlo method, and a model of heat conduction for which the method of finite elements was employed. The numerical model of photothermal signal generation and its experimental validation is described in more detail elsewhere.[11,20] The photothermal signals in Fig. 5 have been calculated to show the effects of μ_a on the response detected by the probe and PPTR. The figure illustrates that an increase in the absorption coefficient of the target results in a faster decay of the photothermal signals. A high μ_a produces a short penetration depth of the excitation light, which heats the target only to a shallow depth but to high peak temperatures. The photothermal signal is then characterized by a large signal peak and a fast decay. Targets with low μ_a allow the excitation light to penetrate deeper, which heats the target at greater depths. The temperature rise in the target and the temperature gradients across the sensing film are smaller and therefore lead to slower signal decay and

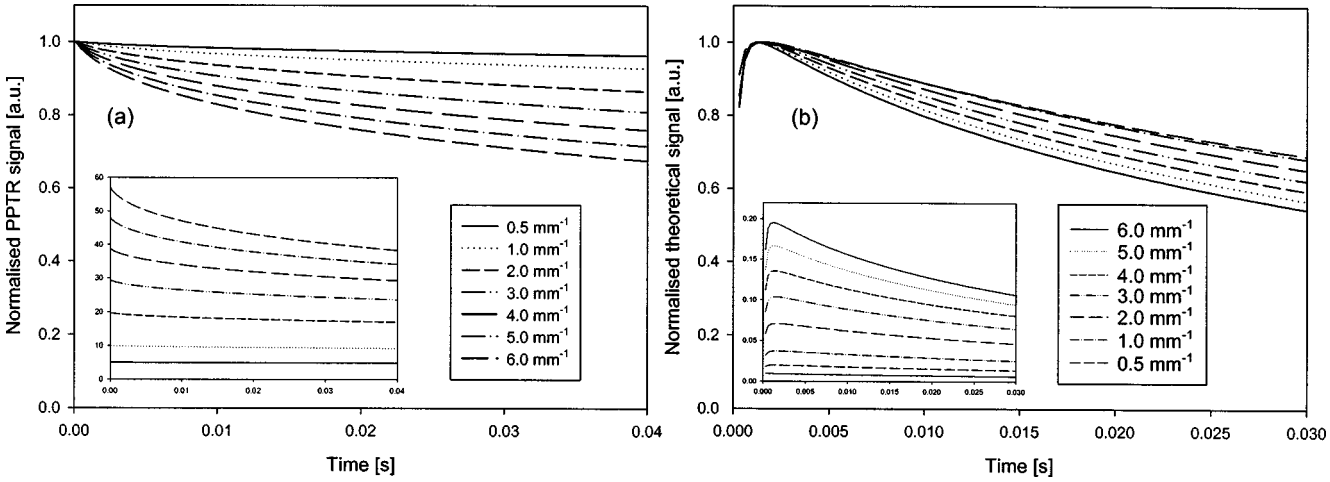

FIG. 5. Effect of μ_a on theoretical (a) PPTR and (b) optical fiber probe signals. An increase in thermal diffusivity would have a similar effect by producing a more rapid decay of the signal. The inset shows the rise in amplitude of the photothermal signal with increasing absorption coefficient.

reduced signal amplitude. Similarly, an increase in thermal diffusivity would produce a faster decay of the photothermal signal.

B. Sensitivity of photothermal signals to optical and thermal parameters

This section investigates which photothermal technique possessed the greatest sensitivity to the optical or thermal coefficients by analyzing the change in the shape of theoretical signals that were normalized to the signal peak. This was achieved by using the numerical model of the photothermal response of the probe and the PPTR analytic model to calculate the tie-dependent sensitivity of the techniques, $S_P(t)$, which was defined as

$$S_P(t) = \frac{dS(t)}{dC} u, \tag{12}$$

where $dS(t)$ is the change in the normalized photothermal signal due to a change in an optical or a thermal coefficient, dC. $dS(t)/dC$ is weighted by u, a fixed perturbation in the coefficient, while all other coefficients are fixed. This calculation was repeated for each coefficient. $dS(t)/dC$ was obtained for all data points of the time-varying signal and for all parameters. Weighting of the photothermal sensitivities with a perturbation of $\pm 10\%$ in all model parameters allowed a direct comparison of $S_P(t)$ produced by the optical and thermal coefficients. The optical coefficients were similar to those found in biological tissue in the visible wavelength region and the thermal coefficients were those of water. The coefficients and uncertainties used to calculate the photothermal sensitivity are listed in Table I. The weighted sensitivities are dependent upon the absolute values of the coefficients for which they are calculated and may vary significantly if the model is very nonlinear. However, in the case of PPTR and the probe, it was found that the models exhibited a nonlinearity of less than 10% over variations in the model parameters of $\pm 50\%$ and therefore allowed a comparison of the different $S_P(t)$. For PPTR, the infrared absorption coefficient μ_{IR} has an influence on the shape of the signal but was not included in the calculation of the photothermal sensitivity because it was found that the effect of variation in μ_{IR} of $\pm 20\%$ could be neglected.

Figures 6(a) and 7(a) show the photothermal sensitivity, i.e., the time-varying change in signal with respect to the signal peak $S_P(t)$ due to a change in an optical or thermal coefficient. The photothermal sensitivity of the optical fiber probe and PPTR shown in Fig. 6(a) demonstrates that both techniques are more sensitive to μ_a than μ_s' PPTR shows greater photothermal sensitivity in general to the optical coefficients than the optical fiber probe. Comparison of Fig. 6(a) to Fig. 7(a) illustrates that the optical fiber probe is more sensitive to the thermal coefficients than μ_a and μ_s' while PPTR is equally sensitive to μ_a than the thermal coefficients. The sensitivity of PPTR to μ_s' is comparable to its sensitivity to the thermal coefficients. According to Figs. 6(a) and 7(a), normalized signals are more sensitive to all coefficients at later times compared to the early part of the signal. Optical and thermal coefficients could, therefore, be determined from the change in the signal with respect to the signal peak. In practice, however, this is not an ideal method since it requires accurate detection of the signal peak and makes the accuracy of the determined coefficients dependent on a small number of data points rather than the entire photothermal signal. A better approach is to fit a model to the entire data set of a non-normalized signal, by multiplying the theoretical signal with an unconstrained amplitude parameter. This would eliminate the need for accurate peak detection. This has been shown to be a more accurate method of determining optical coefficients compared to analyzing normalized signals,[6] since the models are in effect fitted only to the

TABLE I. The optical and thermal coefficients and their uncertainties ($\pm 10\%$) used for the calculation of photothermal sensitivities.

Coefficient	Value	Uncertainty
μ_a (mm^{-1})	1.0	± 0.1
μ_s' (mm^{-1})	2.0	± 0.2
k ($\mathrm{W\,mm^{-1}\,K^{-1}}$)	0.56×10^{-3}	$\pm 0.056\times 10^{-3}$
c ($\mathrm{J\,g^{-1}\,K^{-1}}$)	4.18	± 0.42
ρ ($\mathrm{g\,mm^{-3}}$)	1.0×10^{-3}	$\pm 0.01\times 10^{-3}$

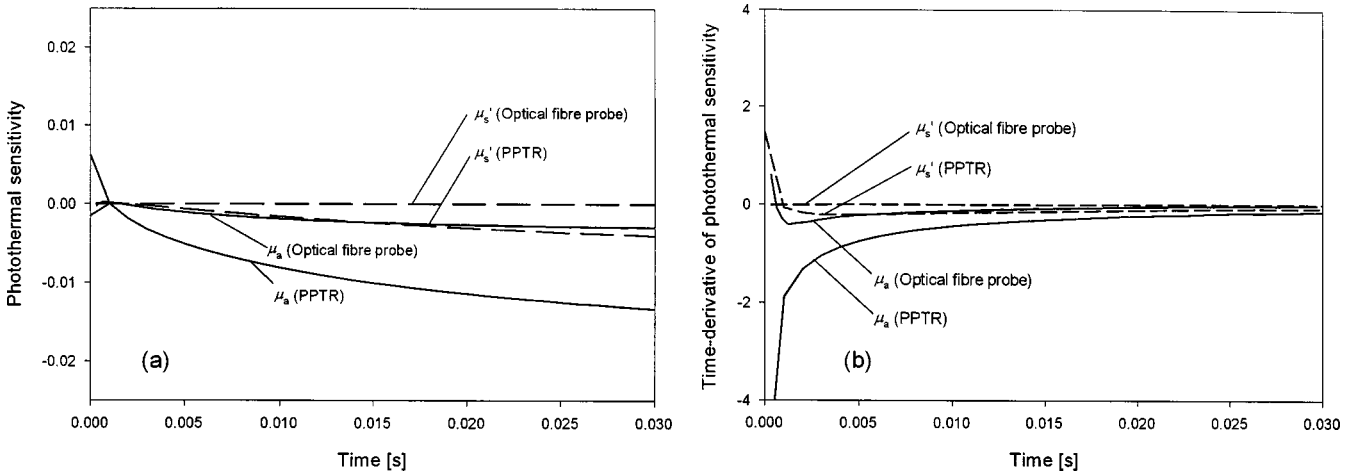

FIG. 6. Photothermal sensitivities (a) of PPTR and the optical fiber probe and their time derivative (b) to the optical coefficients of tissue. (b) illustrates that the signal shape is most affected by μ_a during the early part of a photothermal signal. The effect of μ_s' compared to μ_a on signal shape is much lower for PPTR. μ_s' has no effect on signal shape for the optical fiber probe.

shape of the signal. In order to investigate which part of the photothermal signal is most sensitive to changes in the optical or thermal coefficients, the time derivatives of the photothermal sensitivity were calculated for all coefficients and are shown in Figs. 6(b) and 7(b). The time derivatives provide a measure of the change in the shape of the signal due to a change in the optical and thermal coefficients.

The time derivatives of the photothermal sensitivity shown in Figs. 6(b) and 7(b) illustrate that the shape of the early part of a photothermal signal is most sensitive to changes in the optical and thermal coefficients. This can be explained by the relaxation of the initial temperature gradient, which is determined by the optical and thermal properties. Later parts of the photothermal signal are dominated by the thermal diffusion of a heat source devoid of sharp temperature gradients and therefore largely dependent upon the thermal properties. Figures 6(b) and 7(b) illustrate that the optical and thermal coefficients should be determined by fitting theoretical models to the early part of the photothermal signal. The figures also show that the signal shape is much less affected at later times.

The greater sensitivity of PPTR to μ_a and μ_s' is due to its thermal geometry. In PPTR the area of photothermal excitation is much larger than the area of detection and the radial thermal diffusion length, which results in the detection of heat flow in one spatial dimension perpendicular to the sample surface. The time-dependent cooling of the sample surface is determined by the initial axial temperature gradient, which is dependent upon the optical properties. The axial heat flow is more closely linked to the optical coefficients than the combination of axial and radial heat flow detected by the optical fiber probe. Radial heat flow is solely dependent upon the thermal properties and the geometry of the illuminating beam rather than the optical properties of the target. This results in a reduced sensitivity of the probe to the optical coefficients.

In order to estimate the minimum change in μ_a that each technique can resolve, contour plots of the chi-square residuals between theoretical signals with and without added noise have been calculated. The residuals were obtained from the difference between a theoretical signal and a signal with an added random noise of $\pm 1\%$. The absorption coefficient was $\mu_a = 1.0\ \mathrm{mm}^{-1}$ in both cases. Contour plots were calculated by varying μ_a and an amplitude parameter, with which the signals were multiplied. The amplitude parameter incorporates factors that affect the signal amplitude such as pulse

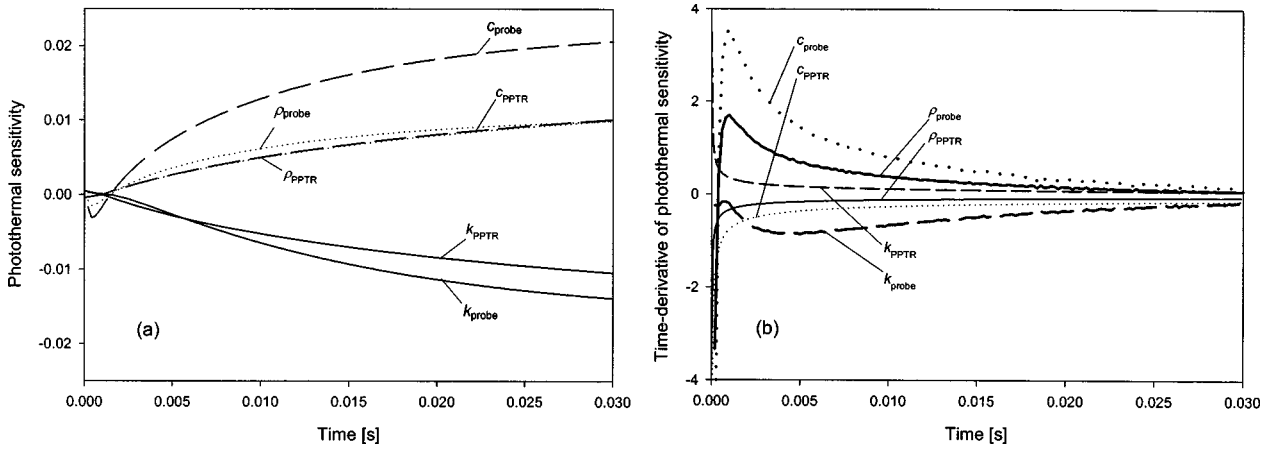

FIG. 7. Photothermal sensitivities of PPTR and the optical fiber probe to the thermal coefficients.

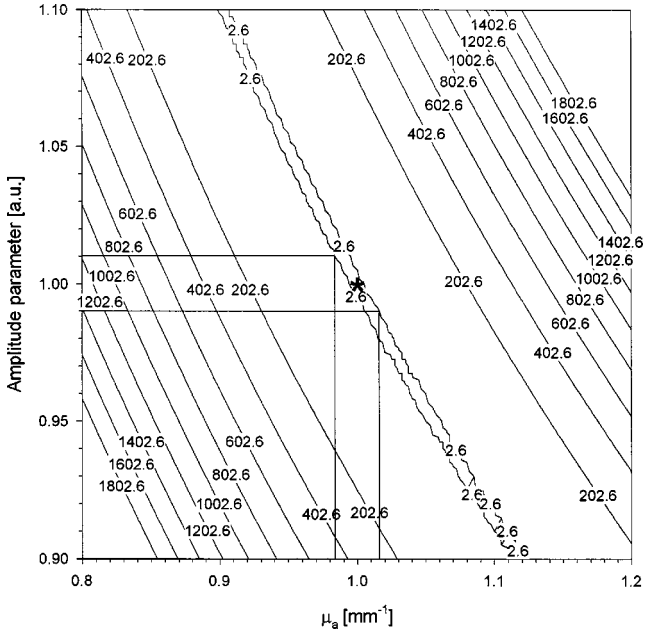

FIG. 8. Contour plot of the residuals between a theoretical PPTR signal with $\pm 1\%$ noise and $\mu_a = 1.0$ mm^{-1} and noiseless theoretical signals. The asterisk represents the minimum residual and best fit to the data. The innermost contour line represents the confidence limit obtained from the noise of the signal. Note that in the case of no prior knowledge in the uncertainty in the scaling factor, the uncertainty in the determined μ_a would be much larger.

energy and system sensitivity and was assumed to have an error equal to the signal noise of $\pm 1\%$.

The uncertainty in the fitted μ_a was estimated from the innermost contour, which represented the chi-square value for $S_{\min}(t) \pm \Delta N$. $S_{\min}(t)$ is the theoretical signal producing the best fit to the data, and hence chi-square minimum, while ΔN is the signal noise at $\pm 1\%$. The intersection of the uncertainty in the amplitude parameter with the innermost contour indicates the uncertainty in μ_a. In the above example, it was found that the absorption coefficient could be determined with a confidence of $\pm 1.5\%$ using PPTR. It can be seen from Fig. 8 that the uncertainty in μ_a would be greater if the uncertainty in the amplitude parameter was known less accurately. If the amplitude parameter was completely unconstrained, the uncertainty in μ_a for the above example would be $\pm 50\%$. The resolution in μ_a produced by the optical fiber probe was lower than PPTR by a factor of 3, further illustrating the probe's lower sensitivity to the optical coefficients. The resolution of the optical coefficients can be further improved by using parameter estimation techniques, which make use of prior knowledge.[11] The sensitivity to the optical coefficients is also dependent upon the value of μ_a. For example, PPTR had a higher μ_a resolution at 5 mm^{-1} because the initial temperature distribution has larger gradients within the thermal diffusion length compared to $\mu_a = 1$ mm^{-1}. Photothermal techniques are, therefore, generally more suited to investigations of highly absorbing materials. Care needs to be taken in the photothermal determination of optical coefficients of tissue. For larger uncertainties in the thermal coefficients of tissue and tissue-like μ_a and μ_s', the effect of the optical coefficients on the photothermal signal may turn out to be almost equal to that of thermal coefficients.

ACKNOWLEDGMENTS

The authors would like to acknowledge the support of the Engineering and Physical Sciences Research Council (EPSRC) who funded this project. The authors would like to thank S. Walker and M. Bluck from the Computational Mechanics Section at Imperial College of Science and Medicine for their help with the numerical model and parameter estimation.

[1] D. P. Almondt and P. M. Patel, *Photothermal Science and Techniques* (Chapman and Hall, London, 1996).
[2] L. C. Aamodt, J. W. Maclachlan Spicer, and J. C. Murphy, J. Appl. Phys. **68**, 6087 (1990).
[3] J. F. Power, Appl. Spectrosc. **45**, 1252 (1991).
[4] A. J. Welch and M. J. C. van Gemert, *Optical-thermal Response of Laser-irradiated Tissue* (Plenum, New York, 1995).
[5] S. L. Jacques, J. S. Nelson, W. H. Wright, and T. E. Milner, Appl. Opt. **32**, 2439 (1993).
[6] S. A. Prahl, I. A. Vitkin, U. Bruggemann, B. C. Wilson, and R. R. Anderson, Phys. Med. Biol. **37**, 1203 (1992).
[7] I. A. Vitkin, B. C. Wilson, and R. R. Anderson, Appl. Opt. **34**, 2973 (1995).
[8] R. M. S. Bindra, R. E. Imhof, A. Mochan, and G. M. Eccleston, J. Phys. (IV), Colloque C7, Suppl. J. Phys. III, **4**, (1994).
[9] T. E. Milner, D. J. Smithies, D. M. Goodman, A. Lau, and J. S. Nelson, Appl. Opt. **35**, 3379 (1996).
[10] F. H. Long, R. R. Anderson, and T. F. Deutsch, Appl. Phys. Lett. **51**, 2076 (1987).
[11] J. G. Laufer, P. C. Beard, S. P. Walker, and T. N. Mills, Phys. Med. Biol. **46**, 2515 (2001).
[12] E. Hecht and A. Zajac, *Optics*, 1st ed. (Addison-Wesley, Reading, MA, 1974).
[13] F. L. Pedrotti and L. S. Pedrotti, *Introduction to Optics*, 2nd ed. (Prentice-Hall, Englewood Cliffs, NJ, 1996).
[14] F. Pérennès, P. C. Beard, and T. N. Mills, Appl. Opt. **38**, 7026 (1999).
[15] T. E. Jenkins, *Optical Sensing Techniques and Signal Processing* [Prentice-Hall International (UK), London, 1987].
[16] E. P. Berg, D. O'Driscoll, and R. E. Imhof, Proceedings of the Photoacoustic and Photothermal Phenomena: 10th International Conference, 1999, pp. 141–143.
[17] P. C. Beard, F. Pérennès, E. Draguioti, and T. N. Mills, Opt. Lett. **23**, 1235 (1998).
[18] H. S. Carslaw and J. C. Jaeger, *Conduction of Heat in Solids* (Oxford University Press, Oxford, 1953), Chap. 2.4, pp. 58–61.
[19] ICI, 'Melinex' datasheet.
[20] J. Laufer, Ph.D. thesis, University College London, 2000.
[21] M. E. P. De Jesus and R. E. Imhof, Appl. Phys. A: Solids Surf. **60**, 613 (1995).
[22] F. H. Long and T. F. Deutsch, IEEE J. Quantum Electron. **QE23**, 1821 (1987).
[23] H. S. Carslaw and J. C. Jaeger, *Conduction of Heat in Solids* (Oxford University Press, Oxford, 1959).